RSC Advances

# MnO2-assisted fabrication of PANI/MWCNT composite and its application in supercapacitor


| | |
|---|---|
| Journal: | *RSC Advances* |
| Manuscript ID: | RA-ART-05-2014-004905.R1 |
| Article Type: | Paper |
| Date Submitted by the Author: | 07-Jul-2014 |
| Complete List of Authors: | Yang, Fan; Institute of Applied Chemistry, Xinjiang University,<br>Xu, Mao-Wen; Institute for Clean Energy & Advanced Materials,<br>Bao, Shu-juan ; Xinjiang University,<br>Sun, Qiang-Qiang; Institute for Clean Energy & Advanced Material, |
| | |

Cite this: DOI: 10.1039/c0xx00000x

www.rsc.org/xxxxxx

ARTICLE TYPE

# $MnO_2$-assisted fabrication of PANI/MWCNT composite and its application in supercapacitor

**Fan Yang[b], Maowen Xu[a], Shu-Juan Bao*[ab], Qiang-Qiang Sun[a]**

***Received (in XXX, XXX) Xth XXXXXXXXX 20XX, Accepted Xth XXXXXXXXX 20XX***

**DOI: 10.1039/b000000x**

Manganese dioxide ($MnO_2$) has been used as a sacrificial template to fabricate polyaniline/multi-walled carbon nanotubes (PANI/MWCNT) composite with core-shell structure through a facile route. The as-synthesized samples have been characterized by Raman spectra, Fourier transform infrared (FT-IR) spectra, field emission scanning electron microscopy (FESEM) and transmission electron microscopy (TEM) for their microstructure and morphology. A series of electrochemical measurements have been performed to study the effects of microstructure and morphology of the samples on their capacitive performance. The results indicate that the as-prepared PANI/MWCNT composite with a core-shell structure provide fast ionic channels for electrochemical energy storage. The maximum specific capacitance of 764 F $g^{-1}$ can be achieved from the hybrid at a current density of 0.25 A $g^{-1}$, and a fairly excellent value of 509 F $g^{-1}$ can be obtained even at a higher current density of 3 A $g^{-1}$.

## 1. Introduction

Under the threat of the rapid depletion of fossil fuels and the increasingly environmental pollution caused by plenty of fossil-fuel consumption, a large number of research efforts have been devoted to exploiting the renewable and clean energy production that can support for the sustainable development of our society[1-3]. Electrochemical capacitors (ECs), usually classified into two categories depending on electrochemical accommodation mechanism as electrochemical double layer capacitors and pseudocapacitors, have been widely used in hybrid electric vehicles and emergency power supplies thanks to their potential to meet the requirements of high power output[1, 4, 5]. As it is commonly known, the capacitive performance of ECs is primarily determined by the adopted electroactive materials. Nowadays, more and more researchers are engaged in designing new materials for the purpose of enhancing the energy density of ECs[6, 7]. New hybrid that can combine faradaic and double layer capacitive performance has made an impressive progress in research on electrode materials[8]. Conducting polymers/carbon components based on composites have aroused intense interest for ECs applications. Polyaniline, as one of the most promising conductive polymers, has been studied extensively since last decade due to its excellent capacity for energy storage and highly electrochemical reversibility[9-11]. Meanwhile, carbon nanotubes (CNTs) with good conductivity have been considered to be shining stars among one-dimensional nanoscale materials [12-14].

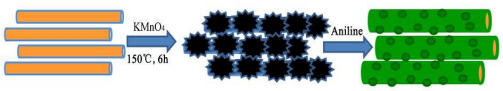


**Scheme 1** Illustration of the process for preparation of PANI/MWCNT hybrid.

Based on the above understanding, the incorporation of CNTs with conducting polyaniline seems to be a prospective attempt to have a synergic effect on improving the performance of ECs. Meng et al. fabricated flexible CNT/polyaniline paper-like films, and the highest specific capacitance 424 F $g^{-1}$ was obtained at discharge current density of 0.2 A $g^{-1}$[15]. Zhou et al. synthesized PANI/MWCNTs composites with core–shell structures as supercapacitor electrode materials with the highest specific capacitance value of 560 F $g^{-1}$ at discharge rate of 2 mV $s^{-1}$[16]. Zhang et al. prepared PANI/MWCNTs composite films by in situ electrochemical polymerization with maximum specific capacitance value of 500 F $g^{-1}$ and poor retention upon cycling [17]. Zhang et al. prepared a PANI/CNTs array composite by electrodeposition with electrochemical capacitance as high as 1030 F $g^{-1}$[18], but the fabrication of vertically aligned carbon nanotube arrays is one of the most complex and expensive techniques.

In our work, $MnO_2$ acted as sacrificial template fabricate PANI/MWCNT hybrid. At the beginning, CNTs were wrapped in $MnO_2$ shell, and then PANI would cover on CNTs to replace $MnO_2$ as the polymerization reaction proceeded. The process for preparation of the hybrid was shown in scheme 1. The electrochemical performance tests demonstrate the PANI/MWCNT hybrid can exhibit a relatively high specific capacitance, rate ability and long-term stability, which make it a competitive candidate as electrode material for future energy storage systems.

## 2. Experimental section

### 2.1 Materials.

Commercial multi-walled CNTs (20 to 50 nm in diameter) were purified by refluxing the as-received sample in nitric acid (10%) for 12 h. Aniline was distilled under vacuum to remove the oxidation impurities before using.

### 2.2 Synthesis of CNT-$MnO_2$.

CNT-$MnO_2$ nanocomposites were synthesized according to a reported reaction[19]. In a typical reaction, suspension of CNTs was prepared by the sonication of acid-treated CNTs (0.1 g) in deionized water (DI water, 20 mL) for about 30 min. 5 mL dissolved with 0.3 g $KMnO_4$ solution was added into the above suspension, and the mixture was magnetic stirred for 2 h, afterwards, the mixed solution was transferred into a 50 mL Teflon-lined stainless-steel autoclave, and treated hydrothermally at 150 °C for 6 h.

### 2.3 Preparation of CNT-PANI.

The preparation process of CNT-PANI was described as follow. In a typical process, suspension A was prepared by dispersing 0.0688 g CNT-$MnO_2$ in 30 mL DI water under ultrasonification. It was then put in an ice bath and stirred slowly. Solution B was prepared by adding 96 μL aniline monomer into the mixed solution of 4.2 mL hydrochloric acid and 15.8 mL DI water. Then B was cooled to room temperature, and mixed with solution A quickly after a while. The polymerization reaction was carried out for 6 h. The resulting green solid product was filtered and washed with DI water and ethanol thoroughly to remove excess ions and monomers. The product was dried in vacuum at 60 °C for 12 h.

### 2.4 General characterization

Raman spectra were recorded using a Bruker Senterra R200-L. Fourier transform infrared (FT-IR) spectra were recorded in the range 400~4000 $cm^{-1}$ on a Thermo Nicolet 6700 FT-IR spectrometer. The morphology and microstructure of the samples were investigated by field-emission scanning electron microscopy (FESEM, JSM-6700F). High-resolution transmission electron microscopy (HRTEM) and was carried out on JEM 2100 microscopes operating at 200 kV.

### 2.5 Electrochemical measurement

The electrodes were fabricated through mixing the active material with 10 wt% conducting black and 5 wt% polytetrafluoroethylene (PTFE) binder of the total electrode mass, and then the mixture was pressed onto SSWM (Stainless Steel Welde Mesh) (1.0 × 1.0 $cm^2$) to make electrodes. Each electrode contains approximately 0.5 mg of active material. Electrochemical characterization was carried out in a conventional three-electrode cell in 1 $mol \cdot L^{-1}$ $H_2SO_4$ electrolytes. Platinum foil and SCE (saturated calomel electrode) were used as the counter and reference electrode, respectively. All electrochemical measurements were conducted using CHI 660 electrochemical workstation (Shanghai Chenhua Co. Ltd., China).

## 3. Results and discussion

Fig. 1a displays the Raman spectra of CNT, CNT-$MnO_2$ and CNT-PANI. The relatively strong peak appeared at a higher wavenumber can be referred to as the G band, which is related to

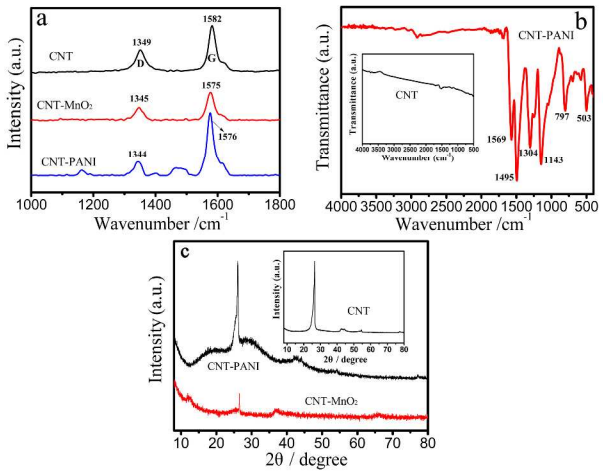


**Fig. 1** (a) Raman spectra of CNT, CNT-$MnO_2$ and CNT-PANI samples; (b) FT-IR of CNT and CNT-PANI samples; (c) XRD patterns of CNT, CNT-$MnO_2$ and CNT-PANI samples.

the graphite $sp^2$ carbon atoms in a two-dimensional hexagonal lattice[20]. The other broad peak can be assigned to the D band, mainly associated with structural defects or disordered carbon structures[21]. Based on the spectra, we can calculate the value of $I_D/I_G$ is 0.85 in CNT and decreases to 0.83 in CNT-$MnO_2$ and 0.23 in CNT-PANI. This variation indicated that the graphitization degree of the hybrid material had increased when moderate $MnO_2$, especially PANI were introduced. In addition, for CNT-PANI, the relatively weak band appeared at 1164 $cm^{-1}$ corresponding to C-H bending of the quinoid ring[22]. The band around 1468-1505 $cm^{-1}$ can be ascribed to C=N stretching mode of the quinoid units[23].

The structures of the CNTs and CNT-PANI were further investigated by FT-IR measurement shown in Fig. 1b. There is no obvious infrared absorption peaks can be observed from pure CNTs. As shown in curve for CNT-PANI, two characteristic bands at 1569 and 1495 $cm^{-1}$ can be assigned to the C=N and C=C stretching of the quinonoid and benzenoid units, indicating the presence of the emeraldine salt state of PANI in the hybrid[24]. Furthermore, the bands around 1304 and 1134 $cm^{-1}$ reveal C–N stretching vibration of the benzene ring and stretching vibration of C=N (-N=quinoid=N-), respectively[10, 25].

Fig. 1c presents the XRD patterns of as-prepared samples. For pure CNTs, the diffraction peaks at 26.5°, 43.2°, 54. 2° and 77.7° can be indexed as the (002), (100), (004) and (110) reflections of graphite, respectively[26]. In comparison, the birnessite-type $MnO_2$ phase[19] can be discovered from the XRD pattern of the CNT-$MnO_2$ composites, whereas the most diffraction peaks from the CNTs have disappeared due to the coating of the $MnO_2$. The as-prepared PANI/CNT composites exhibit a relatively strong reflection of CNTs, which can be assigned to the highly graphitized pristine CNTs.

SEM images with different magnifications are presented in Fig. 2 to observe the morphology and microstructure of as-obtained samples. Clearly, acid-treated CNTs are made of a great number of tubes with different diameter. As we can see from Fig. 2c and d, most CNTs have been wrapped in thick $MnO_2$ "flower shell" consists of many nanoflakes during the hydrothermal

process. It has been demonstrated from Fig. 2e and f that $MnO_2$ could act as good templates for the formation of PANI covered on CNTs.

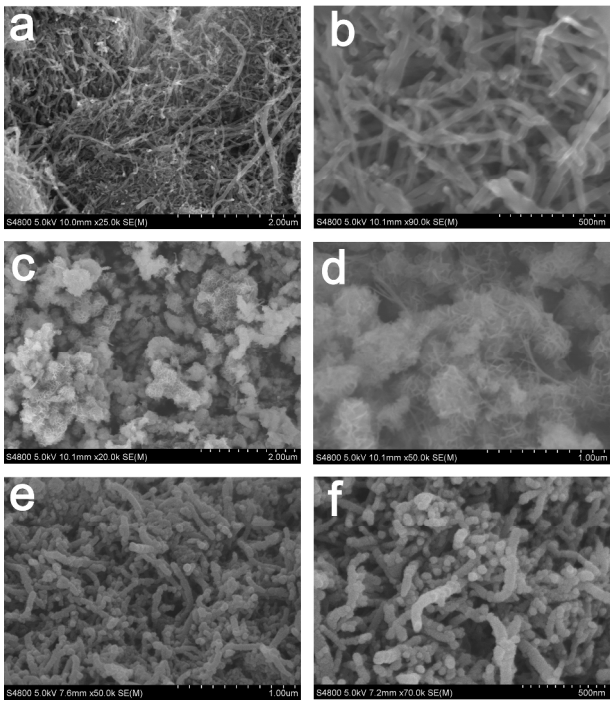


**Fig. 2** Representative SEM images of (a, b) CNT, (c, d) CNT-$MnO_2$ and (e, f) CNT-PANI nanocomposites at different magnifications.

We further conducted TEM to demonstrate the microstructures and morphologies of the samples shown in Fig. 3. It can be seen from Fig. 3a and b that caterpillar-like $MnO_2$ nanoflakes have been successfully anchored on CNTs. Fig. 3c and d indicated that $MnO_2$ shell disappeared and CNTs had been wrapped in PANI shell as the reaction proceeded. In addition, some CNT-PANI composites tubes aggregated during the polymerization process.

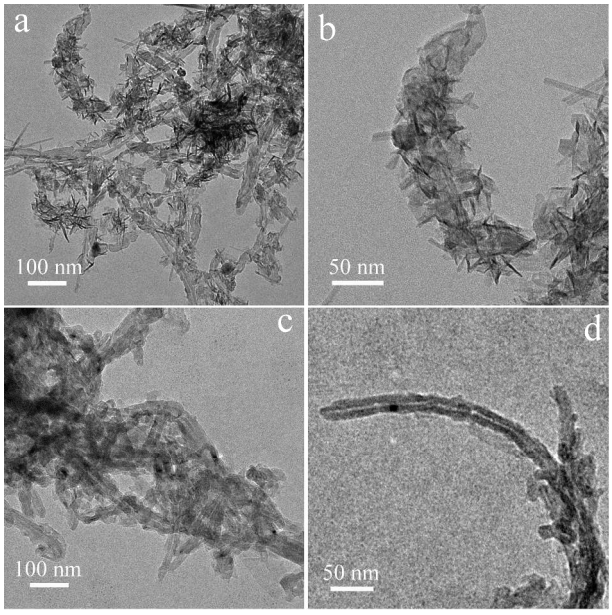


**Fig. 3** TEM images of (a, b) CNT-$MnO_2$ and (c, d) CNT-PANI nanocomposites at different magnifications.

The formation mechanism of CNT-$MnO_2$ in the first step has been reported[19]. Also, it is commonly known that metal oxides such as $MnO_2$, $PbO_2$ and $NH_4VO_3$ can polymerize the aniline due to the charge transfer interaction. When an appropriate amount of aniline monomer was added to the above suspension, the chemical oxidation polymerization would be initiated by reduction of the $Mn^{4+}$ ions and the resulting $Mn^{2+}$ ions would go to the solution[27]. During the polymerization reaction, the $MnO_2$ flakes on CNTs would serve as template and oxidant, where the PANI nucleus could get deposited on. With the reaction prolonging, PANI flakes would cover on CNTs. Meanwhile, the preformed $MnO_2$ would be consumed. Consequently, the CNT-PANI with core-shell hierarchy architecture could be easily produced.

The thermal stability of synthesized CNT-$MnO_2$ and CNT-PANI hybrid material was investigated by TG-DSC. The experiments were carried out in air flow at a heating rate of 10 °C $min^{-1}$ up to 770 °C shown in Fig. 4. For CNT-$MnO_2$, there are three weight loss stages in the TG profile (Fig. 4a), giving a total weight loss of 35.9 wt% up to 770 °C. The mass loss (about 9.3 wt%) in the first stage from room temperature to 200 °C can be attributed to the loss of chemically adsorbed water in the CNT-$MnO_2$ hybrid material[27]. The second apparent weight loss of 17.6 wt% at 300 to 500 °C can be assigned to the transformation of $MnO_2$ to $Mn_2O_3$, identifying with the endothermic peak around 410 °C in the DSC curve. The third weight loss of 9 wt% at 500 to 650 °C can be ascribed to the decomposition of CNTs, which is in keeping with the endothermic peak around 600 °C in the DSC curve. The $MnO_2$ loading in the CNT-$MnO_2$ hybrid material is estimated to be about 64 wt%. Whereas, the TG plot of CNT-PANI shows 100% weight loss at temperatures range from 400 to 770 °C, which clearly demonstrate that $MnO_2$ has been totally consumed during the PANI formation.

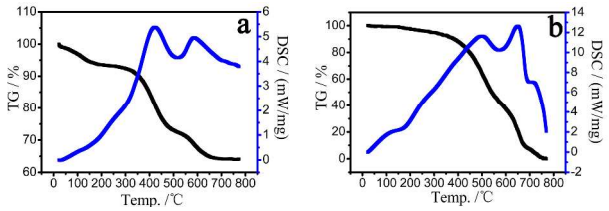


**Fig. 4** TG-DSC plots of (a) CNT-$MnO_2$ and (b) CNT-PANI nanocomposites in air flow at a heating rate of 10 °C $min^{-1}$ up to 770 °C.

The cyclic voltammetry curves of CNT and CNT-PANI electrodes at scan rate of 5 mV $s^{-1}$ are shown in Fig. 5a. The approximately rectangular shape for CNT indicates its electric double layer capacitive character. For CNT-PANI electrodes, two pairs of peaks can be seen at relatively low scan rates: one couple of redox peaks (0.22/0.1 V) are ascribed to the transition of PANI from its leucoemeraldine base (LB) to emeraldine salt (ES) states. The other pair of peaks (0.76/0.73 V) could be attributed to the formation of fully oxidized state of the polymer (pernigraniline). Notably, the symmetrical galvanostatic charge/discharge curves with slight IR drops also imply superior reversible redox reaction and good conductivity (Fig. 5b). Based on the galvanostatic charge/discharge curves, the calculated specific capacitances of CNT-PANI at different current densities from 0.25 to 3 A $g^{-1}$ are summarized in Fig. 5c. As we can see from that the specific capacitance for CNT-PANI electrode decreases with continue increasing the charge/discharge current density. It also manifests

that the highest specific capacitance of 764 F $g^{-1}$ can be achieved from CNT-PANI at a current density of 0.25 A $g^{-1}$, and a fairly excellent value of 509 F $g^{-1}$ can be obtained even at a higher current density of 3 A $g^{-1}$. The cycling stability is considered to be of vital importance for supercapacitor applications. From Fig. 5d, the CNT-PANI displays a good cyclic ability at a current density of 1 A $g^{-1}$. A capacity fade of 11% was observed after 1000 charge/discharge cycles for this hybrid.

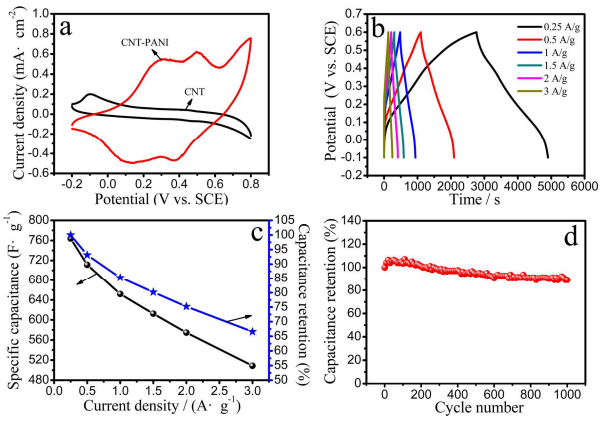


**Fig. 5** (a) Cyclic voltammograms of CNT and CNT-PANI electrodes within the potential window 0 to 0.8 V vs. SCE at 5 mV $s^{-1}$ scan rate in 1 M $H_2SO_4$. (b) Galvanostatic charge/discharge curves of CNT-PANI electrode at different current densities. (c) Multiplying power capacity as a function of discharge current densities of the CNT-PANI electrode. (d) Cycle performance for CNT-PANI electrode at current density of 1 A $g^{-1}$.

## Conclusions

PANI/MWCNT composite with core-shell structure has been successfully fabricated through a facile route. The results indicate that the as-prepared PANI/MWCNT composite with a core-shell structure provide fast ionic channels for electrochemical energy storage. The maximum specific capacitance of 764 F $g^{-1}$ can be achieved from the hybrid at a current density of 0.25 A $g^{-1}$, and a fairly excellent value of 509 F $g^{-1}$ can be obtained even at a higher current density of 3 A $g^{-1}$. Further, the hybrid displays a good cyclic ability.

## Acknowledgments

This work is financially supported by National Natural Science Foundation of China (21163021); Chongqing Key Laboratory for Advanced Materials and Technologies of Clean Energies, Start-up grant under SWU111071 & SWU113077 from Southwest University and Chongqing Science and Technology Commission under cstc2011pt-sy90001 and cstc2012gjhz90002; Natural Science Foundation of Chongqing (cstc2013jcyjA5004); Fundamental Research Funds for the Central Universities (XDJK2013B031).

## Notes and references

[a] *Chongqing Key Laboratory for Advanced Materials and Technologies of Clean Energies, Institute for Clean Energy & Advanced Materials, Faculty of Materials and Energy, Southwest University, Chongqing, 400715, P. R. China. Fax: +86-023-68254969; Tel: +86-023-68254943. E-mail: baoshj@swu.edu.cn*

[b] *Key Laboratory of Material and Technology for Clean Energy, Ministry of Education, Key Laboratory of Advanced Functional Materials, Institute of Applied Chemistry, Xinjiang University, Urumqi 830046, Xinjiang Autonomous Region, P. R. China. E-mail: shjbao@xju.edu.cn*

1. S. Liu, S. Sun and X.-Z. You, *Nanoscale*, 2014, **6**, 2037-2045.
2. F. Wang, S. Xiao, Y. Hou, C. Hu, L. Liu and Y. Wu, *Rsc Adv.*, 2013, **3**, 13059.
3. Z. Weng, H. Guo, X. Liu, S. Wu, K. W. K. Yeung and P. K. Chu, *Rsc Adv.*, 2013, **3**, 24758.
4. C.-Y. Chen, C.-Y. Fan, M.-T. Lee and J.-K. Chang, *J. Mater. Chem.*, 2012, **22**, 7697.
5. X. Zhao, L. Zhang, S. Murali, M. D. Stoller, Q. Zhang, Y. Zhu and R. S. Ruoff, *ACS NANO*, 2012, **6**, 5404.
6. H. Jiang, C. Li, T. Sun and J. Ma, *Chem. Commun (Camb)*, 2012, **48**, 2606.
7. Y. Zhao, J. Liu, Y. Hu, H. Cheng, C. Hu, C. Jiang, L. Jiang, A. Cao and L. Qu, *Adv. Mater.*, 2013, **25**, 591.
8. G. Yu, X. Xie, L. Pan, Z. Bao and Y. Cui, *Nano Energy*, 2013, **2**, 213.
9. W. Fan, C. Zhang, W. W. Tjiu, K. P. Pramoda, C. He and T. Liu, *ACS Appl. Mater. Interfaces*, 2013, **5**, 3382.
10. H.-P. Cong, X.-C. Ren, P. Wang and S.-H. Yu, *Energy & Environmental Science*, 2013, **6**, 1185.
11. M. Liu, Y. E. Miao, C. Zhang, W. W. Tjiu, Z. Yang, H. Peng and T. Liu, *Nanoscale*, 2013, **5**, 7312.
12. Y. Yu, C. Cui, W. Qian, Q. Xie, C. Zheng, C. Kong and F. Wei, *Asia-Pac J. Chem. Eng.*, 2013, **8**, 234.
13. Z. Fan, Z. Qie, T. Wei, J. Yan and S. Wang, *Mater. Lett.*, 2008, **62**, 3345.
14. Y. Hou, Y. Cheng, T. Hobson and J. Liu, *Nano lett.*, 2010, **10**, 2727.
15. C. Meng, C. Liu and S. Fan, *Electrochem. Commun.*, 2009, **11**, 186.
16. Y. Zhou, Z.-Y. Qin, L. Li, Y. Zhang, Y.-L. Wei, L.-F. Wang and M.-F. Zhu, *Electrochim. Acta*, 2010, **55**, 3904.
17. J. Zhang, L.-B. Kong, B. Wang, Y.-C. Luo and L. Kang, *Synthetic Met.*, 2009, **159**, 260.
18. H. Zhang, G. Cao, Z. Wang, Y. Yang, Z. Shi and Z. Gu, *Electrochem. Commun.*, 2008, **10**, 1056.
19. H. Xia, Y. Wang, J. Lin and L. Lu, *Nanoscale Res. Lett.*, 2012, **7**, 33.
20. X. Wen, D. Zhang, L. Shi, T. Yan, H. Wang and J. Zhang, *J. Mater. Chem.*, 2012, **22**, 23835.
21. W. Chen and L. Yan, *Nanoscale*, 2011, **3**, 3132.
22. H. Wang, Q. Hao, X. Yang, L. Lu and X. Wang, *Nanoscale*, 2010, **2**, 2164.
23. W. Chen, R. B. Rakhi and H. N. Alshareef, *J. Phys. Chem. C*, 2013, **117**, 15009.
24. Q. Wang, J. Yan, Z. Fan, T. Wei, M. Zhang and X. Jing, *J Power Sources*, 2014, **247**, 197.
25. D. Zhao, X. Guo, Y. Gao and F. Gao, *ACS Appl. Mater. Interfaces*, 2012, **4**, 5583.
26. Z. Sun, Z. Liu, B. Han, Y. Wang, J. Du, Z. Xie and G. Han, *Adv. Mater.*, 2005, **17**, 928.
27. M. Sathish, S. Mitani, T. Tomai and I. Honma, *J. Mater. Chem.*, 2011, **21**, 16216.